Available online at www.synsint.com

Synthesis and Sintering

ISSN 2564-0186 (Print), **ISSN** 2564-0194 (Online)

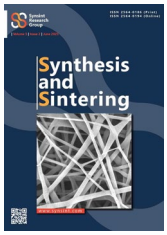

Research article

Green synthesized AgNPs@MSNs reinforced polycaprolactone nanofibers for removal of heavy metals, bacteria, and methylene blue dye from industrial wastewater

Shanli Salahi [a,*], **Sevda Albayrak** [b], **Fevziye Işıl Kesbiç** [c], **Hanifi Çinici** [a]

[a] *Department of Metallurgical and Materials Engineering, Gazi University, Ankara 06500, Turkey*
[b] *Department of Metallurgical and Materials Engineering, Kırıkkale University, Kırıkkale 71450, Turkey*
[c] *Central Research Laboratory, Kuzeykent Campus, Kastamonu University, Kastamonu 37150, Turkey*

A B S T R A C T

This study aims to find solutions to global water scarcity and to address the environmental pollution and serious adverse effects on human health and aquatic ecosystems caused by the inadequacy of conventional water treatment methods. In order to contribute to the solution of these problems, the potential of silver nanoparticles (AgNPs) and mesoporous silica nanoparticles (MSNs) doped nanofibers obtained by the green synthesis method using Betula pendula plant extract in industrial wastewater treatment was investigated. The characterization of the synthesized nanoparticles was carried out in detail using X-ray diffraction (XRD), Fourier transform infrared spectroscopy (FTIR), UV-Vis spectrophotometry, scanning electron microscopy (SEM), and antibiogram tests. The filtration performance of industrial wastewater simulated in a laboratory setting was comprehensively evaluated by atomic absorption spectroscopy (AAS) and UV-spectrophotometry analyses. The characterization of polycaprolactone (PCL) based composite nanofibers produced by electrospinning was carried out by scanning electron microscopy (SEM) and thermogravimetric analysis (TGA). The main findings of the research reveal the successful biosynthesis of silver nanoparticles (AgNPs) with an average diameter of 113 nm and mesoporous silica nanoparticles (MSNs) with an average diameter of 185 nm. Furthermore, AgNPs@MSNs reinforced composite nanofibers provided effective adsorption of heavy metals, organic dyes, and bacterial pollutants found in industrial wastewater. These results indicate that the developed nanofibers have high potential in reducing environmental pollution.

KEYWORDS

Heavy metals
Organic dyes
Green synthesis
Bacterial pollutants
Composite nanofibers
Industrial wastewater

OPEN ACCESS

1. Introduction

The availability of freshwater resources is an essential need for both human settlements and wildlife. Access to potable water plays a critical role in maintaining healthy living conditions and overall well-being. As global water demand continues to increase annually, various types of pollution threaten water resources. Contaminated water sources expose people to pathogens and toxic substances derived from hazardous chemicals, including those used in agricultural irrigation, toxins accumulated in aquatic organisms, and pollutants encountered during recreational activities in contaminated surface waters, leading to serious health risks. In developing countries, direct consumption of contaminated water constitutes one of the major health problems for a large proportion of individuals [1–3].

* Corresponding author. *E-mail address:* shanli.salahi@gazi.edu.tr (S. Salahi)
Received 3 November 2024; Received in revised form 29 June 2025; Accepted 29 June 2025.

https://doi.org/10.53063/synsint.2025.52259

Environmental pollution in developing countries is becoming an increasingly serious problem due to the lack of safe water treatment technologies and limited access to clean drinking water infrastructure. According to the World Health Organization (WHO), 844 million people worldwide lack access to basic drinking water sources, while 230 million people must spend more than 30 minutes per day collecting water from improved water sources, such as rainwater, boreholes, piped water, protected wells, springs, and packaged or transported water supplies [1]. In developing nations, a lack of reliable access to enhanced drinking water supplies significantly increases the probability of waterborne diseases. According to the WHO, approximately 1.6 million people die each year from preventable waterborne diseases such as diarrhea, with 90% of these deaths occurring among children under five [2]. In developing countries, the main concern for human health arises from microbial contamination of drinking water due to pathogens such as bacteria and viruses. In addition, the increasing presence of heavy metals and dyes in water supplies poses a burgeoning concern.

In recent years, the expansion of industrial and urban areas in developing nations has resulted in a significant increase in the presence of pollutants such as heavy metals and dyes in water resources. According to the United Nations, approximately 80% of municipal and industrial wastewater in developing countries is discharged directly into the environment without the necessary treatment processes [3]. Heavy metals are a serious concern due to their inherent toxicity and widely accepted carcinogenic properties, posing significant risks to human health [4–7]. Heavy metal pollution poses a major challenge in the developing world as conventional drinking water treatment methods such as boiling, solar disinfection, and chlorination are inadequate to remove these contaminants [8, 9].

The treatment of wastewater, the recovery of freshwater resources, and their utilization in human activities and agricultural endeavors are of vital importance. As the global water demand increases annually, various types of pollution seriously threaten the quality and availability of water resources [10]. The contamination of wastewater with heavy metal ions and dyes results from various industrial processes such as electroplating, electrolysis, and metal smelting, and from environmental exposure to chemical pollutants. Furthermore, the removal of heavy metals poses a significant health concern due to their carcinogenic and teratogenic properties, leading to various adverse health effects [11]. Therefore, rigorous treatment protocols need to be urgently implemented to ensure the permanent removal of these particles.

Various methodologies are applied to treat wastewater and produce heavy metal-free water. The selection of the appropriate technology depends on its effectiveness in permanently removing heavy metal ions such as arsenic (As), iron (Fe), cadmium (Cd), nickel (Ni), chromium (Cr), cobalt (Co), copper (Cu), and lead (Pb) as well as dyes. Removal of wastes in water treatment can be achieved through adsorption, which is the adhesion of a liquid or gaseous fluid (adsorbate) to a solid surface (adsorbent) through chemical or physical interactions. The adsorption capacity of solid surfaces is affected by the porosity, which determines the interaction of solutes with the adsorbent material. The intermolecular forces resulting from unsaturation significantly increase the binding affinity of solutes, and hence, the adsorption technique has gained wide acceptance due to its practicality, applicability, and efficiency. The adsorption mechanism consists of three sequential stages: migration of the adsorbate from the solution to the adsorbent surface, adhesion to the adsorbent, and subsequent movement along the adsorbent surface [12].

Green synthesis envisages the use of plant extracts as an environmentally friendly alternative to industrial chemicals in the production of nanoparticles. This methodology is preferred over traditional chemical and physical synthesis techniques due to its cost-effectiveness, reduced environmental pollution, and increased safety for both human health and ecological systems [13]. AgNPs have been the focus of extensive interest in the scientific literature due to their significant antimicrobial properties, and many studies have been conducted in this field on their synthesis, characterization, and biological effects [14, 15]. Their importance is not limited to antimicrobial properties, as AgNPs exhibit extraordinary physicochemical, optical, electrical, and magnetic properties that are markedly different from their bulk counterparts [16]. MSNs are greatly appreciated for their highly ordered porous structure, large surface area, and excellent biocompatibility [17–19]. Additionally, nanoparticle biosynthesis via plant-based methodologies stands out as an important area of research that offers a sustainable and biocompatible approach that is compatible with contemporary environmental and biotechnological paradigms [13].

Betula pendula Roth, belonging to the family Betulaceae, is commonly known as white birch, common birch, European white birch, or European silver birch. The species is recognizable by its characteristic white bark and can be a tree or shrub. Betula pendula grows in temperate regions and is distributed throughout Europe, from central Siberia to northern Asia, the southern parts of the Iberian Peninsula, southern Italy, and Greece. This wide geographical distribution results in considerable morphological diversity and has led to the description of many subspecies and cultivars [20–22]. Betula pendula is enriched with various bioactive organic compounds such as procyanidins, terpenes, steroidal compounds, flavonoids, lignans, and catechins. The chemical profile of the extracts varies significantly depending on the particular anatomical parts of the tree, reflecting the diverse phytochemical profile of the species. Differences in the chemical profiles of compounds isolated from the same parts mainly depend on the methodologies used in the isolation process [21, 22].

The scope of this research paper is to investigate the potential of Betula pendula plant extract (BP-Ex) in synthesizing AgNPs and MSNs. Furthermore, the study aims to fabricate AgNPs@MSNs reinforced PCL nanofibers via the electrospinning method and evaluate their efficiency in removing heavy metals, bacterial contaminants, and organic dyes from industrial wastewater. This research will significantly contribute to advancing the application of composite nanofibers in industrial wastewater remediation.

2. Materials and methods

2.1. Preparation of Betula pendula leaf extract (BP-Ex)

Betula pendula leaves were collected and thoroughly washed three times with distilled water before drying. A 10 g sample of the dried leaves was boiled with 100 ml of distilled water for 60 minutes. After this step, the mixture was allowed to cool to room temperature, then filtered and stored at 4 °C.

2.2. Green synthesis of silver nanoparticles (AgNPs)

10 ml of BP-Ex was added to 90 ml of 0.01 M silver nitrate ($AgNO_3$; Merck, 101512) solution and stirred in a hot water bath for 80 minutes to promote the formation of fine-grained AgNPs. The change of solution color from yellow to dark brown was considered as a visual evidence of AgNPs synthesis. Then, the prepared solution was incubated at room temperature in the dark for 24 hours.

The colloidal solution containing the synthesized AgNPs was centrifuged at 12,000 rpm for 20 minutes. After removing the supernatant, the precipitate was washed three times with distilled water and centrifuged again after each wash. In the final step, the precipitate was dried in an oven at 60 °C for 12 hours and then ground into a fine powder.

2.3. Green synthesis of mesoporous silica nanoparticles (MSNs)

At the beginning of the synthesis process, 200 ml of ethanol (C_2H_5OH; Merck, 100983) was transferred into a beaker, and the mixture was placed on a magnetic stirrer. Then, 100 ml of %25 ammonia solution (NH_4OH; Merck, 105432) was added to the mixture, and 6.4 ml of BP-Ex was carefully added. After this step, 10 ml of 0.1 M sodium metasilicate (Na_2SiO_3; TK, 090109) solution was slowly added dropwise to the mixture and the solution was continuously shaken on a magnetic stirrer for 2.5 hours. The change of solution color from transparency to dark reddish brown indicated that MSNs were successfully synthesized. For purification, the colloidal solution containing the synthesized MSNs was centrifuged at 10,000 rpm and 7 °C for 10 minutes. The supernatant was carefully decanted, and then the precipitate was thoroughly washed with ethanol to prepare for the next centrifugation process. The precipitate obtained after centrifugation was dried in an oven at 60 °C for 6 hours to be converted into fine-grained powder form.

2.4. Preparation of simulated heavy metal waste solutions

For solution preparation, 0.1 g of iron (II) sulfate heptahydrate ($FeSO_4.7H_2O$; Merck, 103965), copper (II) sulfate pentahydrate ($CuSO_4.5H_2O$; Merck, 102790), nickel (II) sulfate hexahydrate ($NiSO_4.6H_2O$; Merck, 106727), lead acetate ($C_4H_6O_4Pb.3H_2O$; Zag, 111227), and cobalt (II) sulfate heptahydrate ($CoSO_4.7H_2O$; TK, 200891) were weighed separately and each compound was transferred to appropriate volumetric flasks. Subsequently, a small amount of distilled water was added to each flask, and the solutions were stirred until the solutes were completely dissolved. Finally, each of the simulated heavy metal waste solutions was meticulously prepared by adding distilled water until the total volume became 100 ml, reaching a concentration of 200 ppm, and was continuously stirred.

In the next step, 1 ml of each 200 ppm concentration simulated heavy metal waste solution was taken into separate volumetric flasks. Subsequently, 9 ml of distilled water was added to each flask, and the solutions were mixed thoroughly. As a result of this process, simulated heavy metal waste solutions with a concentration of 20 ppm were obtained in each flask.

In the following stage, 0.5 ml aliquots of each 20 ppm concentration simulated heavy metal waste solution were carefully transferred to separate volumetric flasks. Then, the solutions were diluted by adding 9.5 ml of distilled water to each flask, thus reducing the heavy metal concentration in each solution to 10 ppm.

In the final stage of the simulated heavy metal waste preparation process, 0.25 ml aliquots of each 10 ppm heavy metal solution were meticulously transferred to separate volumetric flasks. Then, the solutions were diluted by adding 9.75 ml of distilled water to each flask, thus reducing the heavy metal concentration to the final level of 1 ppm.

The amount of 0.01 g of MSNs was added to each of the simulated heavy metal solutions prepared at 1 ppm, 10 ppm, and 20 ppm

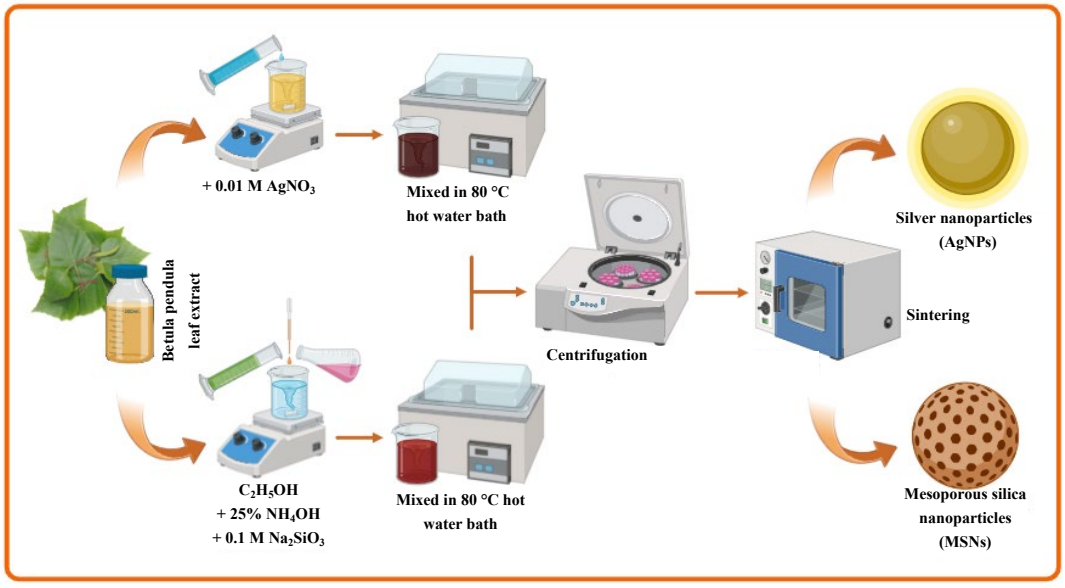

Fig. 1. Schematic representation of the green synthesis procedure of AgNPs and MSNs.

concentrations. The solutions were stirred at 25 °C for 24 hours, then filtered, and the resulting liquids were stored at room temperature. In order to evaluate the heavy metal adsorption performance of MSNs in industrial wastewater, the heavy metal concentrations in simulated standard and purified heavy metal-containing wastewater were measured by AAS, and the results were compared.

2.5. Electrospinning of AgNPs@MSNs reinforced nanofibers

In the formulation phase, 0.5 g of granular Polycaprolactone (PCL; $(C_6H_{10}O_2)_n$; Sigma Aldrich 440744) was added to the mixture prepared by carefully measuring 3.5 ml of acetone (CH_3COCH_3; Merck, 100014) and 1.5 ml of formic acid solution (HCOOH; Merck, 100264) to obtain a homogeneous solution of 10% w/v. In the following step, 0.05 g AgNPs and 0.05 g MSNs were added to this solution. The mixture was transferred to an injector to apply the electrospinning technique for transition to the nanofiber production process. The parameters of the electrospinning device (FYTRONIX) were meticulously set considering the operating voltage of 20 kV, the processing time of 3 hours, the constant flow rate of 1 ml/h, and the distance between the collector and the injector tip of 12 cm. The precise adjustment of these parameters was critical for the successful production of AgNPs@MSNs reinforced nanofibers with the desired properties. Following the production process, the obtained nanofibers were subjected to a stabilization heat treatment at 70 °C for 4 hours.

2.6. Antibiogram analysis methodology

Synthesized AgNPs, MSNs, and pure solutions of $AgNO_3$, BP-Ex were evaluated for antimicrobial susceptibility using agar disc diffusion method against human pathogenic gram-positive Staphylococcus aureus (S. aureus; ATCC 29213) and gram-negative Escherichia coli (E. coli; ATCC 25922) bacteria [23]. The strains were inoculated into Nutrient Broth (Merck, 105443) and incubated at 37 °C for 24 h. After the growth of bacteria, 20 µl of solution was impregnated with sterile blank discs (Bioanalyse) and placed in the Mueller-Hinton Agar (Merck, 103872) plates. Zones of inhibition were measured after 24 hours of incubation at 36 °C. The Vancomycin disc was used as the positive control for S. aureus, whereas the ampicillin disc was used as the positive control for E. coli.

2.7. Preparation of methylene blue dye (MB) contaminated wastewater

The photocatalytic efficiency and dye filtration capacity of the fabricated nanofibers were systematically assessed by monitoring the degradation of methylene blue dye (MB; $C_{16}H_{18}ClN_3S{\cdot}3H_2O$; Carlo Erba) in aqueous solution (pH = 4.3, 6×10^{-3} M initial concentration) under UV lamp (15 W, 254 nm wavelength) irradiation. The MB solution was meticulously prepared by diluting 0.1 ml of MB at a concentration of 6×10^{-6} M with ultra-pure water to achieve a total volume of 100 ml. A 10 ml aliquot of the prepared solution was then carefully transferred into a separate 50 ml beaker with a diameter of 40 mm, accompanied by electrospun nanofibers precisely cut to 10 mm × 10 mm dimensions. The UV lamp was strategically positioned at a distance of 100 mm above the solution surface. The absorbance spectra, indicative of MB degradation, were systematically recorded using a Shimadzu UV/Vis 2600 spectrophotometer, encompassing a photon wavelength range of 400−800 nm, at predefined time intervals of 30, 60, 120, and 180 minutes.

The adsorption spectra of the MB aqueous solutions were recorded using a UV−Vis spectrophotometer over the 400−800 nm wavelength range. The calibration curve, derived from the characteristic absorption peak of MB at 664 nm, yielded a linear equation [24]: $A = 0.1183C + 0.0045$. This equation facilitated the determination of MB concentration (C) in the solution post-photocatalytic treatment.

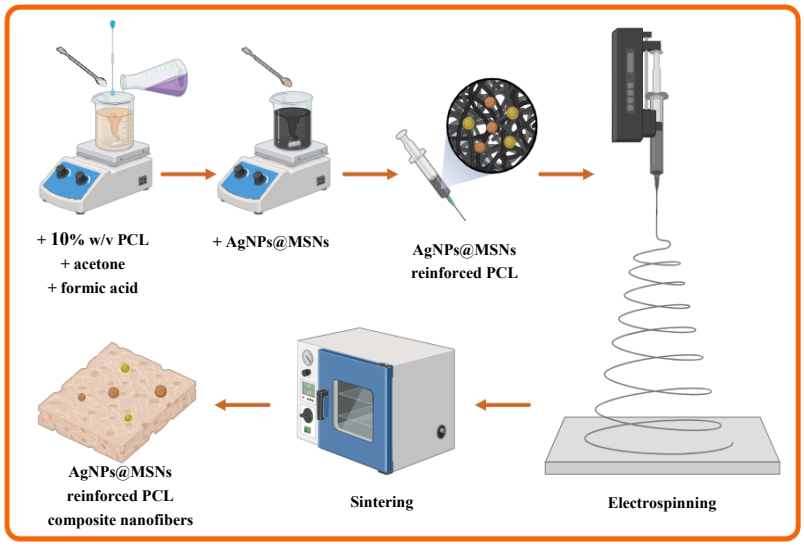

Fig. 2. Schematic representation of the synthesis procedure of AgNPs@MSNs reinforced nanofibers.

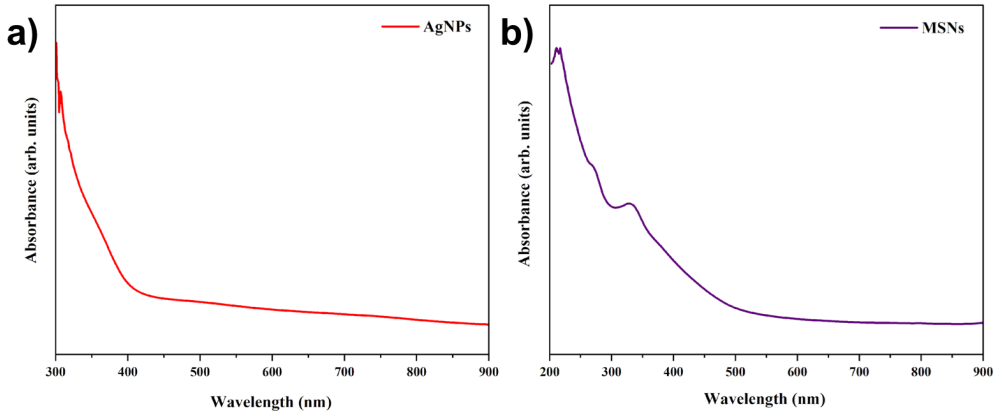

Fig. 3. UV-Vis absorption spectrum of a) AgNPs and b) MSNs.

3. Results and discussion

3.1. UV-Vis absorbance spectroscopy analysis

The incorporation of BP-Ex into silver nitrate solution resulted in a significant change in the color of the solution from yellow to dark brown, indicating the successful synthesis of AgNPs. This color change is due to the characteristic optical properties of AgNPs arise from the excitation of surface plasmon resonance [25, 26]. The surface plasmon resonance (SPR) of the synthesized AgNPs exhibited an absorbance spectrum with a peak at approximately 307 nm using a UV-Vis spectrophotometer (Shimadzu, UV-2600i). This peak, concentrated around 307 nm, clearly reveals that $AgNO_3$ was successfully reduced to silver nanoparticles. This spectral peak, as illustrated in Fig. 3a, not only confirms the rapid biosynthesis of AgNPs but also indicates that the biological reduction process of silver ions initiates at the commencement of the reaction and is completed within a few minutes.

The addition of BP-Ex to a solution containing ethanol, ammonia, and sodium metasilicate led to the successful synthesis of MSNs, which was confirmed by the change in solution color from transparent to dark red-brown. This color change is associated with the excitation of surface plasmon vibrations induced by MSNs. The surface plasmon resonance (SPR) absorption is known to be extremely sensitive to the morphological characteristics of the particles and environmental conditions [27, 28]. A prominent surface plasmon resonance (SPR) peak was observed in the UV-Vis absorption spectrum (Fig. 3b) at a wavelength of approximately 331 nm, indicating the synthesis of MSNs.

3.2. Fourier transform infrared (FTIR) analysis

To investigate the potential adsorption interactions between nanoparticles and impurities in industrial wastewater, binding mechanisms were analyzed using a Bruker VERTEX 70v FTIR spectrometer, operating in the wavelength range of 400–4000 cm^{-1}. In the FTIR spectrum of AgNPs demonstrated in Fig. 5a, prominent absorption peaks were detected at 1575.79 cm^{-1} and 2326.08 cm^{-1}. The peak at 2326.08 cm^{-1} reflects the stretching of the OH group found in alcohol and phenolic compounds, while the peak at 1575.79 cm^{-1} is due to the carbonyl stretching of amide I bonds.

In order to determine the functional groups surrounding the synthesized MSNs, FTIR spectroscopy was applied in the wavelength range of 4000 cm^{-1} to 400 cm^{-1}. As seen in Fig. 5b, the characteristic FTIR spectrum of the nanomaterials reveals the presence of three distinct silica bands in the range of 400 cm^{-1} to 1200 cm^{-1}. The sharp band observed at 457.12 cm^{-1} indicates the bending vibrations of Si–O–Si bonds, while the bands at

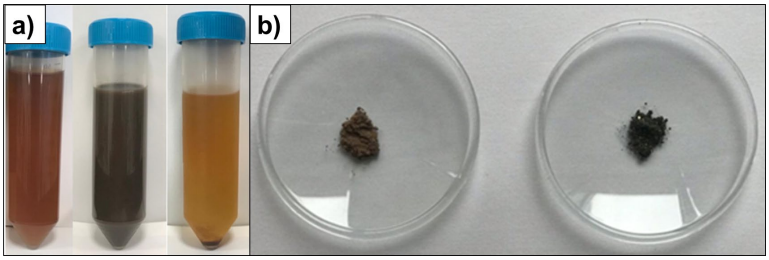

Fig. 4. a) Synthesis of AgNPs and MSNs via colorimetric changes in BP-Ex and b) powdered form of AgNPs and MSNs.

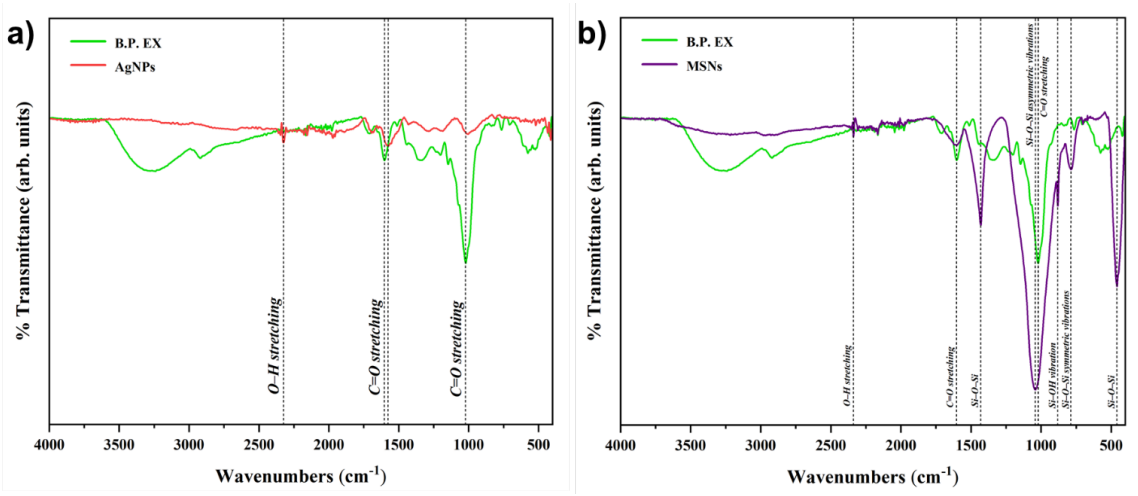

Fig. 5. FTIR spectra of BP-Ex, AgNPs, and MSNs.

785.01 cm^{-1} and 1041.53 cm^{-1} are attributed to the symmetric and asymmetric vibrations of Si–O–Si, respectively. Furthermore, the peak detected at 879.51 cm^{-1} in the spectrum is an absorption indicator reflecting the bending vibration of Si–OH. The peak at 1606.65 cm^{-1} is predicted to originate from the carbonyl stretching of MSNs. The presence of this functional group both increases the stability of the nanoparticles and enhances their potential for biological activity [27, 29].

3.3. X-ray diffraction (XRD) analysis

The XRD analysis using Bruker, D8 ADVANCE X-ray diffractometer revealed prominent diffraction peaks indicating face centered cubic (FCC) crystal structure of AgNPs. The XRD patterns of AgNPs and MSNs correspond to the ICDD 01–071–4612 and ICDD 00–005–0565 PDF cards, respectively. In this study, intense peaks were detected at 38.292 °, 44.508 °, 64.766 °, and 77.809 ° corresponding to (111), (200), (220), and (311) Bragg reflections, respectively. The formation of nanoparticles was supported by the broadening of the Bragg peaks as an indicator of structural changes at the nanoscale.

Moreover, the XRD analysis confirmed the amorphous structure of the synthesized MSNs by the presence of broad peaks observed at 13 ° and 27 ° in the diffraction pattern. The graphical results presented in Fig. 6 play an important role in determining the crystallinity structure type of the synthesized nanoparticles. This observation is in agreement with the existing literature, highlighting the effectiveness of XRD analysis in the characterization of nanoparticles [27, 30, 31].

3.4. Thermogravimetric (TGA) analysis

The thermal degradation behavior of the PCL mixture was systematically determined using a thermogravimetric analyzer (Hitachi, STA 7300), as illustrated in Fig. 7. The TGA curve provides a comprehensive overview of the thermal stability and degradation characteristics of the PCL mixture.

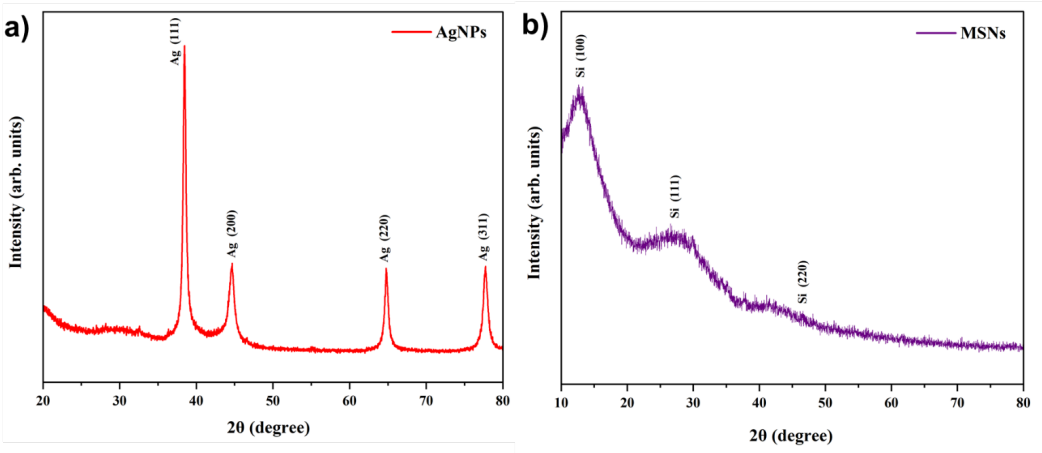

Fig. 6. X-ray diffraction (XRD) patterns of a) AgNPs and b) MSNs.

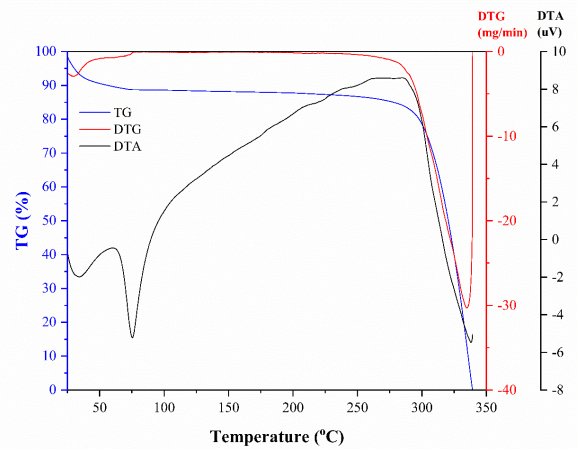

Fig. 7. TGA/DTA thermal analysis diagram for determining the stabilization heat treatment temperature of the produced PCL-based composite nanofibers.

The thermal degradation profile is characterized by a distinct degradation phase between approximately 295 °C and 341 °C. This phase indicates the primary thermal decomposition of the PCL blend. The peak temperature representing the maximum degradation rate was detected at 335 °C. This peak represents the point at which the most rapid mass loss occurs, associated with the degradation of the molecular structure of the polymer.

The thermal behavior of the PCL mixture, as evidenced by the recorded temperature values, aligns closely with the thermal properties documented in existing literature for pure PCL [32–34]. This

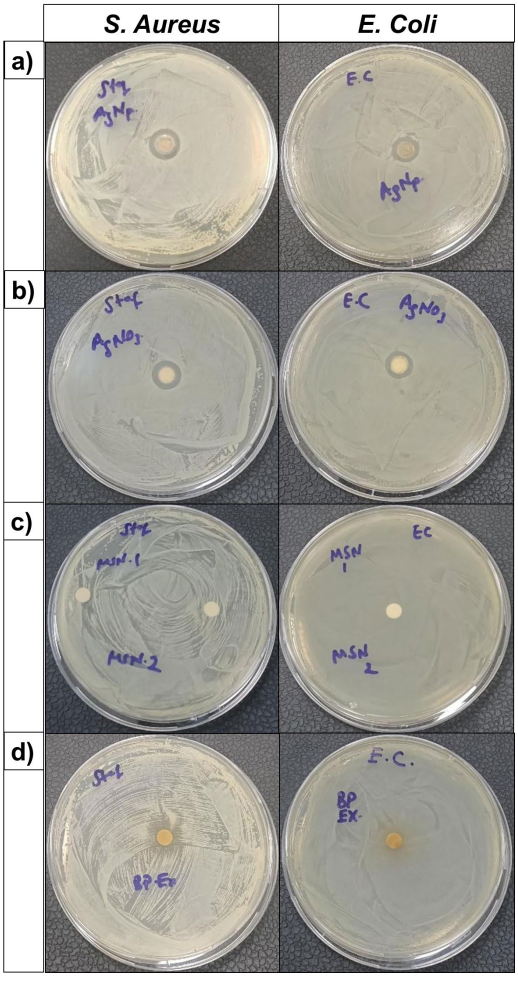

Fig. 8. Antibacterial activity of a) AgNPs, b) $AgNO_3$, c) MSNs, and d) BP-Ex.

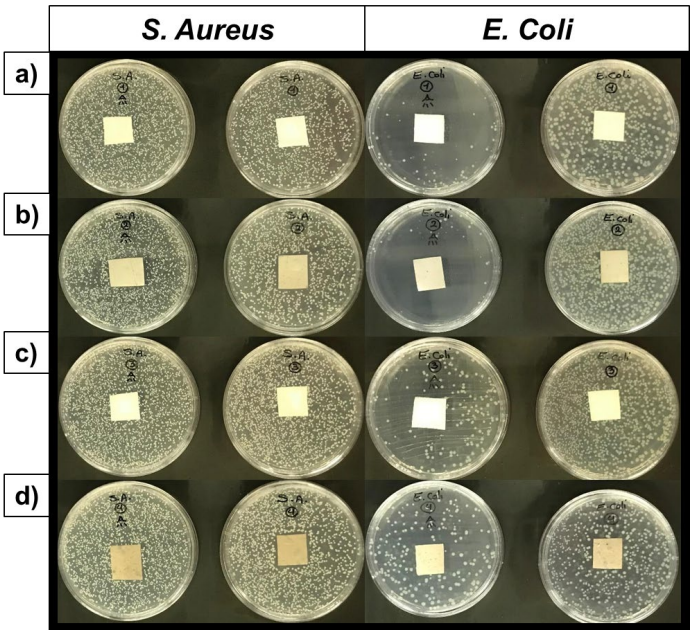

Fig. 9. Antibacterial activity of electrospun nanofibers: a) PCL, b) PCL+AgNPs, c) PCL+MSNs, and d) PCL+AgNPs@MSNs, with an analysis of the effect of light on their effectiveness in the first column of each image.

consistency indicates that the thermal degradation mechanisms and kinetic properties of the PCL mixture are similar to those of pure PCL. The degradation phase and maximum degradation temperature are critical parameters reflecting the stability of the material under thermal stress. In this context, comprehensive thermal analysis confirms that the PCL mixture exhibits thermal properties typical of pure PCL and reinforces the reliability of the experimental procedure employed within this study.

3.5. Antibiogram analysis

3.5.1. Antibacterial efficacy of green synthesized nanoparticles

The antibacterial efficacy of synthesized AgNPs, MSNs, and the pure solution of $AgNO_3$ and BP-Ex was evaluated by measuring the diameter of the inhibition zone (in mm) against S. aureus and E. coli. The disc diffusion test results of solutions against gram-negative and gram-positive human pathogens are given in Fig. 8 and Table 1, respectively.

The results indicate that AgNPs exhibited an inhibition zone of 12 mm against S. aureus and 11 mm against E. coli, demonstrating significant antibacterial activity, although slightly less potent against the gram-negative E. coli. $AgNO_3$ showed an inhibition zone of 12 mm for both S. aureus and E. coli, indicating strong and equivalent antibacterial properties against both bacterial strains. In contrast, MSNs did not exhibit any antibacterial activity against either S. aureus or E. coli, as evidenced by a 0 mm zone of inhibition. BP-Ex demonstrated the highest antibacterial activity against S. aureus with an inhibition zone of 13 mm, surpassing both AgNPs and $AgNO_3$, but showed no antibacterial activity against E. coli. These results suggest that silver-based materials (AgNPs and $AgNO_3$) are effective against both gram-positive and gram-negative bacteria [13, 35], while BP-Ex is highly effective against S. aureus but ineffective against E. coli.

3.5.2. Antibacterial efficacy of electrospun nanofibers

The antibacterial efficacy of electrospun nanofibers, including 1: PCL, 2: AgNPs-doped PCL, 3: MSNs reinforced PCL, and 4: AgNPs@MSNs reinforced PCL, was assessed by measuring the diameter of inhibition zones (in mm) against S. aureus and E. coli. Detailed results from disc diffusion tests against gram-negative and gram-positive human pathogens are documented in Fig. 9 and Table 2.

The antibiogram analysis of produced nanofibers reveals that PCL+AgNPs nanofibers exhibit significant antibacterial activity, demonstrated by a zone of inhibition measuring 27 mm against S. aureus and 19.5 mm against E. coli. This indicates effectiveness against both gram-positive and gram-negative bacteria. Notably, PCL+AgNPs@MSNs nanofibers showed enhanced antibacterial performance with an inhibition zone of 27.6 mm against S. aureus and 20 mm against E. coli, suggesting that the combination of AgNPs with MSNs enhances the antibacterial efficacy of the nanofibers. In contrast, the control groups, which included pure PCL and PCL+MSNs nanofibers, did not exhibit any antibacterial activity against either bacterial strain, as evidenced by a 0 mm inhibition zone.

These results underscore the pivotal role of AgNPs in conferring antibacterial properties to the nanofibers. The slightly reduced efficacy against E. coli compared to S. aureus can be attributed to the inherent differences in the cell wall structures of gram-positive and gram-negative bacteria, with the latter possessing an outer membrane that can act as an additional barrier to antibacterial agents [13, 35]. Overall, the findings suggest that AgNPs doped PCL-based nanofibers (PCL+AgNPs and PCL+AgNPs@MSNs) are effective antimicrobial agents against both gram-positive and gram-negative bacteria, offering potential applications in environmental fields where antibacterial materials are essential.

Table 1. Inhibition zone (mm) of prepared samples against test strains.

Sample	S. aureus (gram-positive)	E. coli (gram-negative)
AgNPs	12	11
$AgNO_3$	12	12
MSNs	0	0
BP-Ex	13	0

Table 2. Inhibition zone (mm) of nanofibers against test strains.

Nanofibers	S. aureus (gram-positive)	E. coli (gram-negative)
PCL	0	0
PCL+AgNPs	27	19.5
PCL+MSNs	0	0
PCL+AgNPs@MSNs	27.6	20

3.6. Scanning electron microscope (SEM) analysis

3.6.1. SEM analysis of green synthesized nanoparticles

Field-emission scanning electron microscopy (Hitachi FE-SEM, SU8700) micrographs of the synthesized AgNPs and MSNs at the 500 nm scale are presented in Fig. 10. These images reveal that both AgNPs and MSNs produced by the green synthesis method exhibit a homogeneous distribution throughout the sample and have a distinct circular morphology, aligning with the results reported in the literature [13, 27, 36].

3.6.2. SEM analysis of electrospun nanofibers

Scanning electron microscope (Thermo Scientific SEM, Particle-X) micrographs of electrospun PCL, PCL+AgNPs, PCL+MSNs, and PCL+AgNPs@MSNs composite nanofibers at 3 μm and 1.5 μm scales are presented in Fig. 11, respectively. The distinct and well-defined morphology, along with the homogeneous distribution of the nanofibers, provides crucial evidence for the successful outcome of the optimization process [36, 37].

3.7. Energy dispersive x-ray spectroscopy (EDS) analysis

3.7.1. EDS analysis of green synthesized nanoparticles

The EDS analysis was performed to determine the elemental composition of the green synthesized nanoparticles. The obtained EDS spectrum shows a distinct peak corresponding to silver (Ag) with 87.0 wt% in AgNPs (Fig. 12a), confirming the successful synthesis and high purity of AgNPs [13]. Furthermore, the low standard deviation value (±0.4) accompanying this peak emphasizes the homogeneity of the nanoparticles and the consistency of the synthesis process. In addition, the spectrum shows peaks at 9.5 wt% and 3.6 wt% for carbon (C) and oxygen (O), respectively. The presence of carbon is attributed to the plant extract used in the green synthesis process, and the organic compounds in the extract are known to act as both reducing and stabilizing agents. The detected oxygen may be due to partial oxidation of the nanoparticles or may be considered as a result of organic capping agents derived from the plant extract.

The EDS analysis presented in Fig. 12b, performed on MSNs, revealed a prominent silicon (Si) peak at 24.0 wt% and a prominent oxygen (O) peak at 54.5 wt%. The low standard deviation values observed for Si (±0.2) and O (±0.4) elements indicate a high degree of homogeneity and regularity in the silica structure. Furthermore, the carbon (C) peak at 21.5 wt% is consistent with the plant extract used during the synthesis. The detected carbon content may be due to the residues of organic compounds in the extract. Therefore, EDS analysis confirms that both high-purity AgNPs and MSNs were successfully synthesized via the plant extract-based green synthesis method [27].

3.7.2. EDS analysis of electrospun nanofibers

The EDS analysis was performed to reveal the elemental composition of the electrospun nanofibers and the obtained spectra are presented in Fig. 13. The EDS spectrum of pure Polycaprolactone (PCL) nanofibers (Fig. 13a) shows dominant peaks corresponding to carbon (C) and oxygen (O) elements, which are the main components of PCL. The detected characteristic peaks are located at approximately 0.28 keV and 0.53 keV energy levels, respectively. In addition, the absence of any other peaks in the spectrum confirms the chemical purity of PCL nanofibers and reveals that there is no evidence of contamination or addition of any foreign elements. The EDS spectrum of AgNPs reinforced PCL nanofibers (Fig. 13b) reveals the presence of additional element peaks, especially silver (Ag), with prominent signals at around 3 keV and 22 keV. The presence of these silver peaks confirms that AgNPs have been successfully integrated into the nanofiber matrix. Furthermore, the detection of nitrogen (N) at approximately 0.39 keV

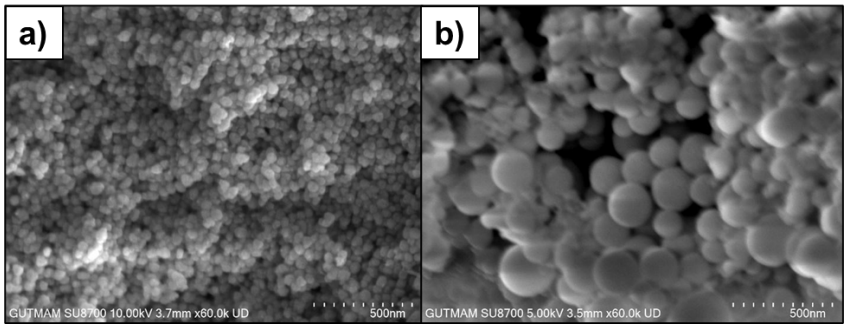

Fig. 10. SEM images of the green synthesized nanoparticles: a) AgNPs, b) MSNs.

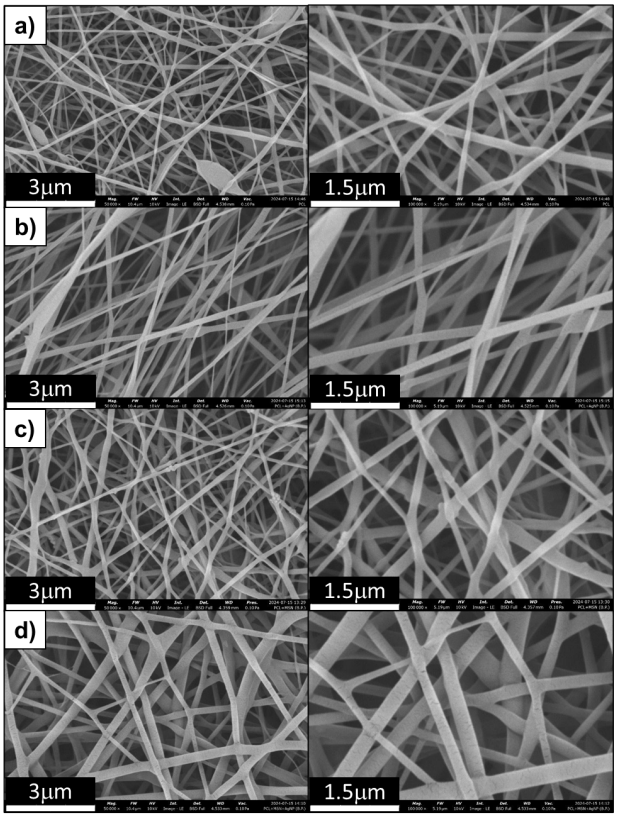

Fig. 11. SEM micrographs of electrospun nanofibers: a) PCL, b) PCL+AgNPs, c) PCL+MSNs, and d) PCL+AgNPs@MSNs.

is most likely attributed to the residual stabilizers used during the synthesis of AgNPs, indicating the presence of trace amounts of nitrogen in the composite nanofibers.

The EDS spectrum of PCL nanofibers loaded with MSNs (Fig. 13c) exhibits a prominent silicon (Si) peak at approximately 1.74 keV in addition to carbon and oxygen peaks. This Si signal unequivocally confirms the successful integration of MSNs into the PCL nanofiber matrix. Furthermore, the absence of any unexpected elemental peaks in the spectrum highlights the chemical purity and structural integrity of the composite nanofibers.

The EDS spectrum of PCL nanofibers reinforced with AgNPs and MSNs (Fig. 13d) presents a combination of characteristic peaks observed in the PCL+AgNPs and PCL+MSNs spectra. The spectrum clearly shows the presence of carbon, oxygen, silicon, and silver elements, with the Si peak appearing at 1.74 keV and Ag peaks at around 3 keV and 22 keV. These findings unequivocally confirm that both MSNs and AgNPs have been successfully loaded into the PCL matrix. Furthermore, the nitrogen peak at 0.39 keV was observed again, which is probably due to the residual nitrogen used during AgNPs synthesis. All these results confirm that the nanoparticles were effectively loaded into the electrospun PCL nanofibers and are homogeneously distributed within the polymer matrix [36, 37]. Comprehensive analysis of EDS spectra confirms the successful fabrication of high-purity and homogenous PCL-based composite nanofibers and clearly highlights their potential in advanced applications.

3.8. Dynamic light scattering (DLS) analysis

The size distribution and polydispersity properties of AgNPs obtained by the green synthesis method were investigated in detail by Malvern, Zetasizer Nano ZS90 DLS analyzer, as shown in Fig. 14. As a result of this analysis, the Z-Average diameter of AgNPs was determined to be 113.4 nm. This value is an important parameter in determining the average size of nanoparticles and is accepted as a quantitative measure of the general morphological properties of the sample. The polydispersity index (PdI) was recorded as 0.194, which indicates that the size variability between nanoparticles is minimal and therefore has a moderately narrow size distribution. In DLS studies, a PdI value below 0.2 generally indicates the presence of a monodisperse system. In this case, it is understood that the heterogeneity between the sizes of the synthesized nanoparticles is low and is kept in a homogeneous structure [27, 37].

The density-weighted size distribution analysis detects a distinct peak at 142.4 nm, which accounts for 99.1% of the total density. This indicates that the majority of nanoparticles are concentrated around this size. In addition, a secondary peak at 26.31 nm with only a 0.9% contribution indicates the presence of smaller-sized nanoparticles in the sample. The absence of additional peaks or significant scattering for larger sizes implies that the nanoparticles exhibit minimal agglomeration, thus providing a homogeneous distribution. The graphical representation of the density-based size distribution supports these findings with a distinct and sharp narrow peak around 142.4 nm. This distribution highlights the high uniformity of the nanoparticles,

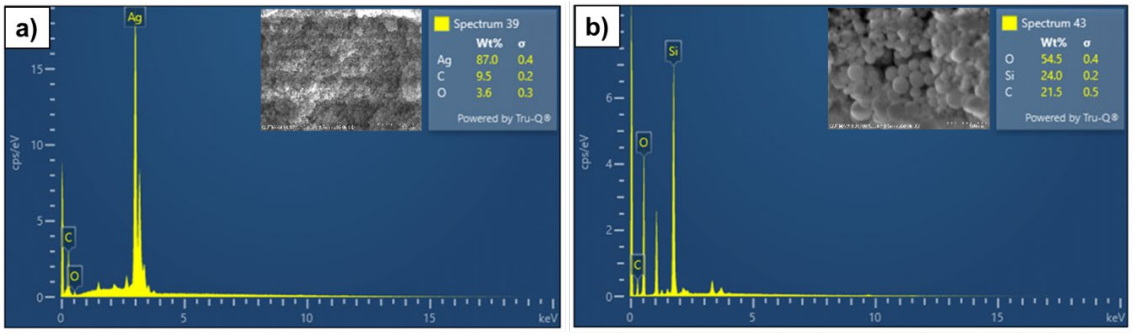

Fig. 12. EDS analysis of the green-synthesized nanoparticles: a) AgNPs, b) MSNs.

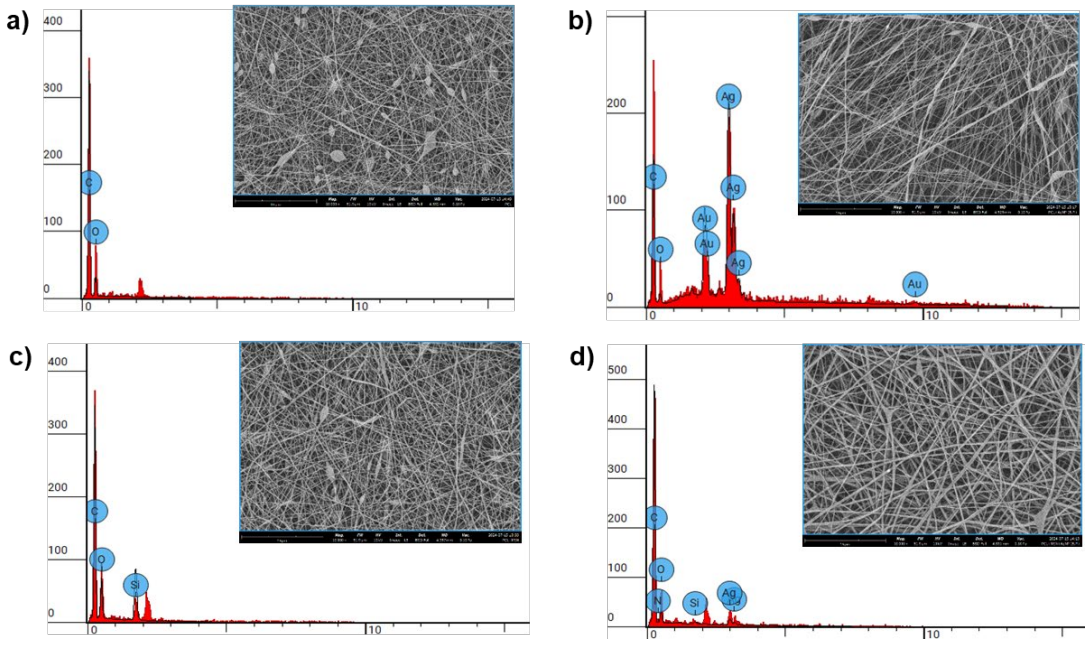

Fig. 13. EDS analysis of electrospun nanofibers: a) PCL, b) PCL+AgNPs, c) PCL+MSNs, and d) PCL+AgNPs@MSNs.

which is critical to ensure consistent performance in subsequent applications. In addition, the small size distribution data is also consistent with the observations, as 50% of the nanoparticles were found to be below 129 nm and 90% below 233 nm. These results provide strong evidence of a narrow size distribution and support the effective performance of the nanoparticles in their potential applications.

The derived count rate of 190,546.4 kcps reinforces the accuracy of the DLS measurements as an indicator of a high signal-to-noise ratio. This high count rate indicates that the scattering signal is strong enough to allow accurate size analysis. Overall, the DLS analysis confirms the successful production of AgNPs with a narrow size distribution and limited agglomeration, demonstrating the effectiveness of the green synthesis method used. These results highlight that AgNPs exhibit

Cumulant Results		Distribution Results				Undersize Results	
Z-Average (nm):	113,4	Size (d.nm):	% Int	σ	%Pd	Di (%)	Size (d.nm):
Pd Index:	0,194	Peak 1: 142,4	99,1	62,26	43.7	50	129
Polydispersity (nm):	49.9	Peak 2: 26,31	0,9	4,733	18.0	90	233
%Polydispersity:	44,0	Peak 3: 0,000	0,0	0,000	0	95	268
Derived kcps:	190546,4						

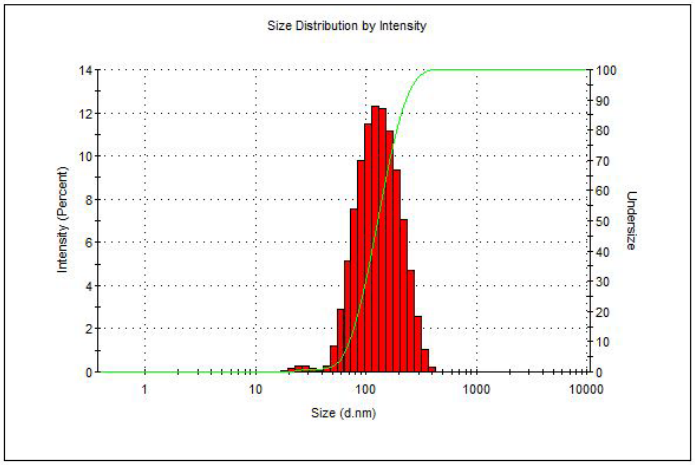

Fig. 14. DLS analysis of AgNPs.

superior performance in potential applications where the size uniformity of nanoparticles plays a critical role in terms of reproducibility and efficiency.

The data obtained from DLS analysis of MSNs synthesized by the green method, presented in Fig. 15, provide deep insights about the size distribution and polydispersity of the sample. Z-Average, determined as 184.8 nm, is a basic parameter expressing the density-weighted average hydrodynamic diameter of the nanoparticles in the suspension. The PdI was recorded as 0.332, indicating that the size variation among MSNs is relatively under control, but contains some heterogeneity. Despite this, the overall size distribution analysis reveals that the synthesized nanoparticles exhibit a reasonably uniform structure [27]. The size distribution profile reveals that the majority of the green synthesized MSNs form a well-defined and homogeneous population with a prominent peak where 99.2% of the intensity is concentrated around 168.0 nm. This distribution indicates that the synthesis process has consistently concentrated the majority of the nanoparticles within a certain size range. However, the secondary peak at 5272 nm, which has a contribution of only 0.8%, indicates the presence of aggregations that may have occurred during the synthesis process. This peak is likely to have occurred as a result of the formation of larger nanoparticle clusters, indicating the presence of heterogeneous structures in a limited portion of the synthesis.

The density distribution plot confirms the high uniformity of the main nanoparticle population with a sharp and distinct peak located around 168.0 nm. This finding indicates that the synthesis concentrated the majority of nanoparticles around this size, while the small secondary peak at 5272 nm indicates the presence of rare larger clusters. Although this may minimally affect the overall uniformity, the overall undersize distribution data further illustrates this trend. The data reveal that 50% of the nanoparticles are below 160 nm and 90% below 247 nm, further reinforcing the clear dominance of the primary population around 168.0 nm despite the polydispersity.

The derived count rate was recorded as 4588.4 kcps, which is lower than expected for denser or homogeneous samples, but remains at a sufficient level to ensure the reliability of DLS measurements. This decrease in count rate can be attributed to a decrease in particle concentration or a decrease in scattering efficiency, possibly as a result of the presence of larger aggregates.

3.9. Atomic atomic absorption spectroscopy (AAS) analysis

The results of AAS analysis of heavy metals such as Pb, Ni, Cr, Fe, and Cu using a fast sequential atomic absorption spectrometer (AA240FS) analyzer obtained for MSNs reveal that 100% of the heavy metals initially present at <3 ppm levels in simulated industrial wastewater samples were removed. The findings highlight the superior heavy metal removal capability of MSNs, indicating their promise as an efficient solution for environmental water remediation.

3.10. UV-Vis spectroscopic analysis of methylene blue dye (MB) filtration by nanofibers

The UV-Vis absorbance spectra of MB solutions, demonstrated in Fig. 16, exhibit significant differences after exposure to various nanofiber composites, clearly revealing the changes in the adsorption capacities of the synthesized nanomaterials. The spectra show the main absorbance peak of MB at approximately 664 nm, which serves as a critical parameter to quantitatively determine the remaining dye concentration in the solution. The modest decrease in absorbance observed in the spectrum of MB solution after 180 minutes of interaction with pure PCL nanofibers reflects the limited adsorption capacity of the unmodified form of the PCL matrix, indicating the low binding ability of pure PCL nanofibers towards the dye.

It was found that AgNPs doped PCL nanofibers provided an increase in absorption at 664 nm wavelength, which indicates a higher adsorption efficiency. This improvement is attributed to the plasmonic properties

Cumulant Results		Distribution Results				Undersize Results	
Z-Average (nm): 184,8		Size (d.nm):	% Int	σ	%Pd	Di (%)	Size (d.nm):
Pd Index: 0,332	Peak 1:	168,0	99,2	53,55	31.9	50	160
Polydispersity (nm): 106.6	Peak 2:	5272	0,8	425,3	8.1	90	247
%Polydispersity: 57,7	Peak 3:	0,000	0,0	0,000	0	95	283
Derived kcps: 4588,4							

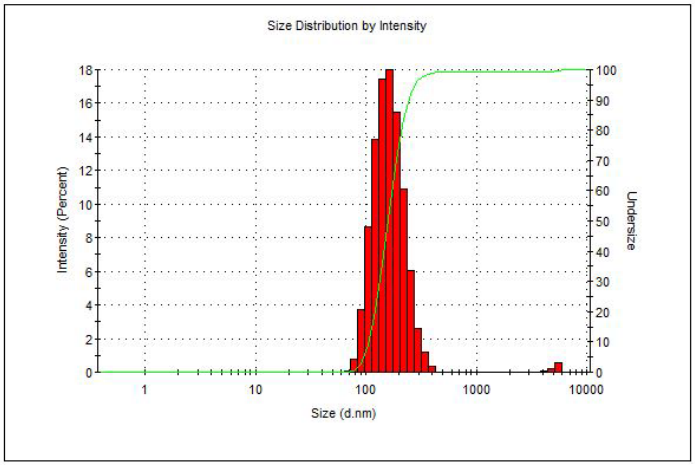

Fig. 15. Dynamic light scattering (DLS) analysis of MSNs.

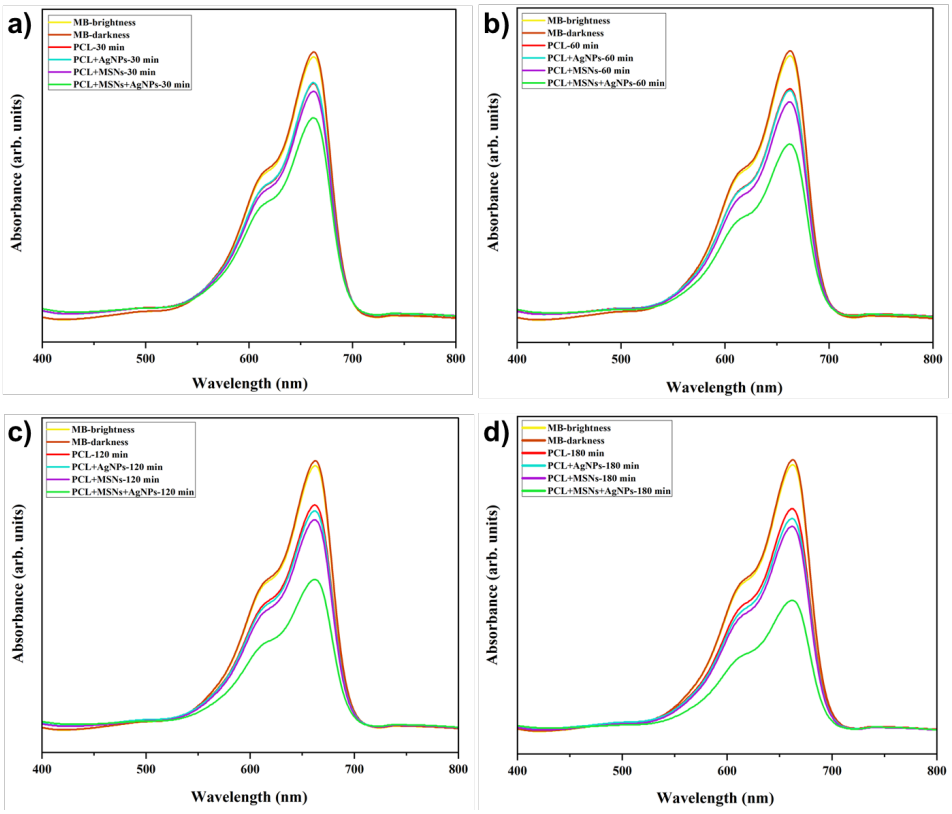

Fig. 16. UV-Vis absorbance spectra of different nanofiber composites obtained after exposure to MB solutions for a) 30 minutes, b) 60 minutes, c) 120 minutes, and d) 180 minutes were analyzed. The investigated composites were pure PCL nanofibers, PCL composite nanofibers reinforced with silver nanoparticles (PCL+AgNPs), PCL composite nanofibers reinforced with mesoporous silica nanoparticles (PCL+MSNs), and PCL nanofibers enriched with both silver nanoparticles and mesoporous silica nanoparticles (PCL+AgNPs@MSNs). In addition, MB-brightness and MB-darkness spectra were used as control samples representing the original MB solution.

of AgNPs, which both accelerate catalytic degradation and enhance the adsorption of MB molecules via localized surface plasmon resonance (LSPR) effect [38, 39]. The integration of MSN into the PCL matrix resulted in a significant decrease in the adsorption behavior, demonstrating the superior adsorption potential of MSNs. This improved adsorption performance is attributed to the large surface area, complex pore structure, and easily functionalizable surface chemistry of MSNs. These structural features provide an efficient adsorption mechanism by offering a large number of active sites for the adsorption of MB molecules.

Composite nanofibers reinforced with AgNPs@MSNs showed the most significant decrease in absorbance, thus revealing the synergistic interaction between these two nanoparticles. This synergy is most likely due to the simultaneous effects of both catalytic and adsorptive mechanisms. AgNPs increase the degradation rate of MB, while MSNs optimize this process with their high adsorption capacity. The significant decrease in absorbance rate of PCL+AgNPs@MSNs composite nanofiber at 664 nm exhibits superior efficiency in MB removal, making this composite nanofiber the most efficient adsorbent system within the scope of the study. These findings highlight the decisive role of functionalization of nanoparticles in improving the adsorptive properties of PCL nanofibers and provide important scientific implications for the design and development of high-performance nanocomposites for the treatment of dye-contaminated wastewater [40, 41].

4. Conclusions

Experimental findings demonstrate that AgNPs and MSNs were successfully produced by the biological synthesis method using BP-Ex, proving that this method offers an environmentally friendly, rapid and cost-effective approach. SEM analyses reveal that the average diameter of the synthesized AgNPs is approximately 113 nm, while the average diameter of MSNs is approximately 185 nm, confirming that both nanoparticles exhibit a spherical morphology. Furthermore, SEM micrographs confirmed the successful fabrication of nanofibers and revealed that the nanoparticles exhibited a homogeneous distribution in the synthesized AgNPs@MSNs doped PCL nanofibers. These results indicate that in addition to the structural integrity of the doped composite nanofibers, the nanoparticles were effectively integrated into the PCL matrix, resulting in a distribution that could enhance the overall performance of the nanocomposite. Antibiogram test results revealed that AgNPs@MSNs reinforced PCL nanofibers showed high antibacterial activity, especially on S. aureus. These findings highlight the positive effect of nanoparticles on bacterial inhibition and their potential application areas. In addition, AAS results showed that heavy metal content in simulated industrial wastewater samples containing <3 ppm heavy metals were completely, 100% removal efficiency, removed. Moreover, AgNPs@MSNs reinforced PCL nanofibers demonstrated superior efficiency in removing MB due to the

synergistic catalytic and adsorptive effects of the nanoparticles. This highlights the critical role of nanoparticle functionalization in enhancing the adsorptive properties of PCL nanofibers for effective dye-contaminated wastewater treatment. These findings show that AgNPs@MSNs reinforced PCL nanofibers can provide environmentally friendly, effective, and economical solutions. In conclusion, these studies provide an important foundation for the potential of green nanotechnology. Such approaches have the potential to revolutionize industrial processes while promoting environmental sustainability.

CRediT authorship contribution statement

Shanli Salahi: Investigation, Conceptualization, Methodology, Data curation, Project administration, Writing – original draft.
Sevda Albayrak: Investigation, Methodology, Data curation, Writing – original draft.
Fevziye Işıl Kesbiç: Investigation, Methodology, Visualization, Validation, Writing – original draft.
Hanifi Çinici: Project administration, Supervision, Funding, Writing – review & editing.

Data availability

All data presented in the study are included in the manuscript. No additional data or supplementary materials are available.

Declaration of competing interest

The authors declare that they have no known competing financial interests or personal relationships that could have appeared to influence the work reported in this paper.

Funding and acknowledgment

Extend our sincere gratitude to the Gazi University Scientific Research Projects (GÜ BAP) Unit for providing an academic grant under Project ID No. 8961.
Gazi University funded all the chemicals used in the research.

References

[1] WHO, Guidelines for drinking‐water quality fourth edition incorporating the first addendum, Who Chron. 38 (2017) 104–108.
[2] A.B. Pandit, J.K. Kumar, Clean Water for Developing Countries, Annu. Rev. Chem. Biomol. Eng. 6 (2015) 217–246. https://doi.org/10.1146/annurev-chembioeng-061114-123432.
[3] U.N. Water, 2018 UN world water development report, nature-based solutions for water, United Nations. (2018).
[4] S. Chakraborty, A.R. Dutta, S. Sural, D. Gupta, S. Sen, Ailing bones and failing kidneys: a case of chronic cadmium toxicity, Ann. Clin. Biochem. Int. J. Lab. Med. 50 (2013) 492–495. https://doi.org/10.1177/0004563213481207.
[5] K.M. Gleason, L. Valeri, A.H. Shankar, M.O.S.I. Hasan, Q. Quamruzzaman, et al., Stunting is associated with blood lead concentration among Bangladeshi children aged 2-3 years, Environ. Heal. 15 (2016) 103. https://doi.org/10.1186/s12940-016-0190-4.
[6] L. Järup, Hazards of heavy metal contamination, Br. Med. Bull. 68 (2003) 167–182. https://doi.org/10.1093/bmb/ldg032.
[7] J.R. Schwartzbord, E. Emmanuel, D.L. Brown, Haiti's food and drinking water: A review of toxicological health risks, Clin. Toxicol. 51 (2013) 828–833. https://doi.org/10.3109/15563650.2013.849350.
[8] M. de Kwaadsteniet, P.H. Dobrowsky, A. van Deventer, W. Khan, T.E. Cloete, Domestic Rainwater Harvesting: Microbial and Chemical Water Quality and Point-of-Use Treatment Systems, Water, Air, Soil Pollut. 224 (2013) 1629. https://doi.org/10.1007/s11270-013-1629-7.
[9] J. Chaudhary, G. Tailor, M. Yadav, C. Mehta, Green route synthesis of metallic nanoparticles using various herbal extracts: A review, Biocatal. Agric. Biotechnol. 50 (2023) 102692. https://doi.org/10.1016/j.bcab.2023.102692.
[10] H. Genç-Fuhrman, P.S. Mikkelsen, A. Ledin, Simultaneous removal of As, Cd, Cr, Cu, Ni and Zn from stormwater using high-efficiency industrial sorbents: Effect of pH, contact time and humic acid, Sci. Total Environ. 566–567 (2016) 76–85. https://doi.org/10.1016/j.scitotenv.2016.04.210.
[11] J.-C. Lee, Y.-O. Son, P. Pratheeshkumar, X. Shi, Oxidative stress and metal carcinogenesis, Free Radic. Biol. Med. 53 (2012) 742–757. https://doi.org/10.1016/j.freeradbiomed.2012.06.002.
[12] T.A. Saleh, Protocols for synthesis of nanomaterials, polymers, and green materials as adsorbents for water treatment technologies, Environ. Technol. Innov. 24 (2021) 101821. https://doi.org/10.1016/j.eti.2021.101821.
[13] S. Salahi, T. Ghaffari, Antibacterial efficacy of green-synthesized silver nanoparticles from rosemary, pennyroyal, and eucalyptus extracts against E. coli and S. aureus bacteria, Synth. Sinter. 4 (2024) 101–107. https://doi.org/10.53063/synsint.2024.42218.
[14] O. Pryshchepa, P. Pomastowski, B. Buszewski, Silver nanoparticles: Synthesis, investigation techniques, and properties, Adv. Colloid Interface Sci. 284 (2020) 102246. https://doi.org/10.1016/j.cis.2020.102246.
[15] F.K. Alsammarraie, W. Wang, P. Zhou, A. Mustapha, M. Lin, Green synthesis of silver nanoparticles using turmeric extracts and investigation of their antibacterial activities, Colloids Surf. B: Biointerfaces. 171 (2018) 398–405. https://doi.org/10.1016/j.colsurfb.2018.07.059.
[16] M.I. Bruce, Metal Clusters in Chemistry—Bibliography of Reviews 1988–1997, Metal Clusters in Chemistry, John Wiley & Sons, Ltd. (1999) 1711–1754. https://doi.org/10.1002/9783527618316.ch6.
[17] V. Ambrogi, A. Donnadio, D. Pietrella, L. Latterini, F.A. Proietti, et al., Chitosan films containing mesoporous SBA-15 supported silver nanoparticles for wound dressing, J. Mater. Chem. B. 2 (2014) 6054–6063. https://doi.org/10.1039/C4TB00927D.
[18] Á. Szegedi, M. Popova, K. Yoncheva, J. Makk, J. Mihály, P. Shestakova, Silver- and sulfadiazine-loaded nanostructured silica materials as potential replacement of silver sulfadiazine, J. Mater. Chem. B. 2 (2014) 6283–6292. https://doi.org/10.1039/C4TB00619D.
[19] J. Liu, S. Li, Y. Fang, Z. Zhu, Boosting antibacterial activity with mesoporous silica nanoparticles supported silver nanoclusters, J. Colloid Interface Sci. 555 (2019) 470–479. https://doi.org/10.1016/j.jcis.2019.08.009.
[20] B. Demirci, K.H.C. Başer, F. Demirci, M.T. Hamann, New Caryophyllene Derivatives from Betula litwinowii, J. Nat. Prod. 63 (2000) 902–904. https://doi.org/10.1021/np990438g.
[21] D. de Rigo, G. Caudullo, T.H. Durrant, J. San-Miguel-Ayanz, The European Atlas of Forest Tree Species: modelling, data and information on forest tree species, Publications Office of the European Union. (2016). https://doi.org/10.2788/038466.
[22] M.S. Vladimirov, V.D. Nikolić, L.P. Stanojević, L.B. Nikolić, A.D. Tačić, Common birch (Betula pendula Roth.): Chemical composition and biological activity of isolates, Adv. Technol. 8 (2019) 65–77. https://doi.org/10.5937/SavTeh1901065V.
[23] S. Guzmán, M. G. Dille, J. Godet, Synthesis of silver nanoparticles by chemical reduction method and their antibacterial activity, Int. J. Mater. Metall. Eng. 2 (2008) 100–107. https://doi.org/10.5281/zenodo.1062628.
[24] M.P. Gonullu, D.D. Cakil, C. Cetinkaya, Influence of thermal treatment and Fe doping on ZnO films by ultrasonic spray pyrolysis,

Thin Solid Films. 793 (2024) 140265. https://doi.org/10.1016/j.tsf.2024.140265.
[25] A. Saha, N. Giri Kumar, S. Agarwal, Silver nanoparticle based hydrogels of Tulsi extracts for tropical drug delivery, Int. J. Ayurveda Pharma Res. 5 (2017) 17–23.
[26] P. Mulvaney, Surface Plasmon Spectroscopy of Nanosized Metal Particles, Langmuir. 12 (1996) 788–800. https://doi.org/10.1021/la9502711.
[27] M. Abbasi, R. Gholizadeh, S.R. Kasaee, A. Vaez, S. Chelliapan, et al., An intriguing approach toward antibacterial activity of green synthesized Rutin-templated mesoporous silica nanoparticles decorated with nanosilver, Sci. Rep. 13 (2023) 5987. https://doi.org/10.1038/s41598-023-33095-1.
[28] S. Mosleh-Shirazi, M.A.J. Kouhbanani, N. Beheshtkhoo, S.R. Kasaee, A. Jangjou, et al., Biosynthesis, simulation, and characterization of Ag/AgFeO2 core–shell nanocomposites for antimicrobial applications, Appl. Phys. A 127 (2021) 857. https://doi.org/10.1007/s00339-021-05005-7.
[29] S. Majeed, M. Danish, N.A. Zakariya, R. Hashim, M.T. Ansari, et al., In Vitro Evaluation of Antibacterial, Antioxidant, and Antidiabetic Activities and Glucose Uptake through 2-NBDG by Hep-2 Liver Cancer Cells Treated with Green Synthesized Silver Nanoparticles, Oxid. Med. Cell. Longev. 2022 (2022) 1646687. https://doi.org/10.1155/2022/1646687.
[30] B. Purnawira, H. Purwaningsih, Y. Ervianto, V.M. Pratiwi, D. Susanti, et al., Synthesis and characterization of mesoporous silica nanoparticles (MSNp) MCM 41 from natural waste rice husk, IOP Conf. Ser. Mater. Sci. Eng. 541 (2019) 12018. https://doi.org/10.1088/1757-899X/541/1/012018.
[31] A. Mourhly, M. Khachani, A. El Hamidi, M. Kacimi, M. Halim, S. Arsalane, The Synthesis and Characterization of Low-Cost Mesoporous Silica SiO2 from Local Pumice Rock, Nanomater. Nanotechnol. 5 (2015) 35. https://doi.org/10.5772/62033.
[32] L.M. Lozano-Sánchez, I. Bagudanch, A.O. Sustaita, J. Iturbe-Ek, L.E. Elizalde, et al., Single-Point Incremental Forming of Two Biocompatible Polymers: An Insight into Their Thermal and Structural Properties., Polymers (Basel). 10 (2018) 391. https://doi.org/10.3390/polym10040391.
[33] R.A. Khan, A.J. Parsons, I.A. Jones, G.S. Walker, C.D. Rudd, Preparation and Characterization of Phosphate Glass Fibers and Fabrication of Poly(caprolactone) Matrix Resorbable Composites, J. Reinf. Plast. Compos. 29 (2010) 1838–1850. https://doi.org/10.1177/0731684409337554.
[34] A. López-Cervantes, I. Domínguez-López, J.D.O. Barceinas-Sánchez, A.L. García-García, Effects of surface texturing on the performance of biocompatible UHMWPE as a bearing material during in vitro lubricated sliding/rolling motion., J. Mech. Behav. Biomed. Mater. 20 (2013) 45–53. https://doi.org/10.1016/j.jmbbm.2012.12.010.
[35] S. Salahi, Removal of Heavy Metals & Bacterial Infection from Industrial Wastewater Using Nanocomposite of Silver Nanoparticles & Household Wastes, International Students Scientific Conference, TalentDetector, Poland. (2023) 586–592.
[36] M. Tavira, M. Mousavi-Khattat, Z. Shakeran, A. Zarrabi, PCL/gelatin nanofibers embedded with doxorubicin-loaded mesoporous silica nanoparticles/silver nanoparticles as an antibacterial and anti-melanoma cancer, Int. J. Pharm. 642 (2023) 123162. https://doi.org/10.1016/j.ijpharm.2023.123162.
[37] M.A. Jadidi Kouhbanani, S. Mosleh-Shirazi, N. Beheshtkhoo, S.R. Kasaee, S. Nekouian, et al., Investigation through the antimicrobial activity of electrospun PCL nanofiber mats with green synthesized Ag–Fe nanoparticles, J. Drug Deliv. Sci. Technol. 85 (2023) 104541. https://doi.org/10.1016/j.jddst.2023.104541.
[38] S.M. El-Bahy, J. Arshad, S. Munir, K. Chaudhary, D. Alhashmialameer, et al., Improved photocatalytic performance of a new silver doped BiSbO4 photocatalyst, Ceram. Int. 48 (2022) 23914–23920. https://doi.org/10.1016/j.ceramint.2022.05.062.
[39] E.S. Gad, K. Chaudhary, A.H. Ahmed, S. Rafiq, A.M. Yousif, M. Suleman, Hydrothermal synthesis of bifunctional Ag/MnO2 nanowires decorated with V2O5 nanorice: Photocatalytic and electrochemical impedance study for treatment of impurities present in waste water, Opt. Mater. (Amst). 135 (2023) 113274. https://doi.org/10.1016/j.optmat.2022.113274.
[40] A. Cordoba, M. Guernelli, M. Montalti, C. Saldías, M.L. Focarete, A. Leiva, Nanofibers of chitosan-polycaprolactone blends as active support for photocatalytic nanoparticles: Outstanding role of chitosan in the degradation of an organic dye in water, Int. J. Biol. Macromol. 253 (2023) 127111. https://doi.org/10.1016/j.ijbiomac.2023.127111.
[41] Y. Cheng, C. Xia, H.A. Garalleh, M. Garaleh, N.T. Lan Chi, K. Brindhadevi, A review on optimistic development of polymeric nanocomposite membrane on environmental remediation, Chemosphere. 315 (2023) 137706. https://doi.org/10.1016/j.chemosphere.2022.137706.